Acta of Bioengineering and Biomechanics
Vol. 27, No. 1, 2025

Original paper
DOI: 10.37190/ABB-02563-2024-03

The effect of restricted ankle dorsiflexion on knee injury risk during landing

ZANNI ZHANG[1], DATAO XU[1, 2], MEIZI WANG[1, 3], HUIYU ZHOU[1], MINJUN LIANG[1], JULIEN S. BAKER[1], YAODONG GU[1]*

[1] Faculty of Sport Science, Ningbo University, Ningbo, China.
[2] Faculty of Engineering, University of Pannonia, Veszprem, Hungary.
[3] Department of Biomedical Engineering, Faculty of Engineering, Hong Kong Polytechnic University, Hong Kong SAR, China.

Purpose: This study utilized a combination of musculoskeletal modeling and finite element analysis to investigate the effects of varying ankle dorsiflexion ranges on knee joint loading, soft tissue stress distribution, and the coactivation patterns of muscles surrounding the knee during landing. *Methods*: Based on the Weight-Bearing Lunge Test (WBLT), a total of 32 basketball players into two groups: normal dorsiflexion (ND) and limited dorsiflexion (LD) and conducted six countermovement jumps (CMJ) while collecting motion and force data. Personalized musculoskeletal models were created using OpenSim to analyze kinematics and kinetics, and Helium-free MRI and CT scans were used for finite element modeling to assess internal tissue stress in the knee. *Results*: During landing, the patellofemoral joint contact force in LD was reduced compared to the ND. The coactivation of muscles around the knee joint decreased. The von Mises stress in the tibial cartilage, meniscus, anterior cruciate ligament and posterior cruciate ligament were elevated. *Conclusions*: The results suggest that increased ankle dorsiflexion during landing may effectively reduce internal tissue stress in the knee joint while enhancing muscle coactivation around the knee joint and increasing patellofemoral joint contact force. These findings provide valuable theoretical support for strategies to reduce the risk of knee injuries during landing. Additionally, they offer reliable technical approaches and theoretical insights for studying injury mechanisms in other sports activities, such as running and lateral jumping.

Key words: *ankle dorsiflexion, landing injury, finite element analysis, helium-free MRI, opensim, musculoskeletal modeling*

1. Introduction

During the performance of high-intensity sports, especially basketball, where activities such as jumping and rapid movements are integral, injuries to the lower limbs are among the most prevalent types of injury sustained by athletes [33], the cause of this damage is largely due to excessive impact force [16]. The ankle joint, as the first movable joint in contact with the ground, is one of the key anatomical structures that reduces the impact force on the lower limbs in jumping sports. Ankle motion plays a crucial role in sports performance and injury risk [76], especially during jumping and landing. Ankle function directly affects the knee and hip joints' movement pattern and load distribution.

The dorsiflexion ability of the ankle joint not only impacts on an athlete's ability to jump but is also closely linked to stability during landing. During jumping movements, the landing phase imposes significant demands on joint impact forces and muscle coordination. Insufficient ankle function can increase energy demands on the proximal joints [35], [72]. During landing, the knee joint, which serves as a critical link between the ankle and hip, is highly vulnerable to injury [24], [74]. Existing studies suggest that increasing the angle of ankle plantarflexion during landing may reduce the impact forces transmitted to the knee joint, thereby decreasing the risk of injury to the medial femoral attachment of

* Corresponding author: Yaodong Gu, Faculty of Sport Science, Ningbo University, Ningbo, China. E-mail: guyaodong@nbu.edu.cn
Received: December 11th, 2024
Accepted for publication: February 19th, 2025

the anterior cruciate ligament (ACL) [64]. Additionally, reduced ankle mobility in basketball players has been shown to contribute to patellar joint pain [1], [61]. Healthy female athletes typically exhibit a larger dynamic range of motion (ROM) during takeoff and landing. Conversely, limited ankle dorsiflexion is linked to a higher risk of injury during jump landing activities. Adjusting the initial ankle contact angle has been suggested as a potential strategy to reduce knee joint injury risk [49]. Repeated exposure to high-impact forces on the knee can result in non-contact ACL injuries, meniscal damage, and cartilage injuries.

Among the many jumping tests used in medical and performance evaluation, the Countermovement Jump (CMJ) test, widely used to assess explosive power and lower limb biomechanics, has become a standard tool in sports medicine and biomechanical research [52]. The CMJ test effectively simulates jumping and landing movements typically seen in sports scenarios [48]. Previous studies have compared the effects of squat jumps and CMJ at different starting positions on athletic performance, revealing that CMJ utilizes rebound force more efficiently, resulting in higher jump heights [21]. Power output and explosive force can be optimized by adjusting the starting position and movement speed, thereby enhancing jump performance [45]. While various factors influencing CMJ landing have been explored, the impact of ankle dorsiflexion ROM on lower limb biomechanics during CMJ has not received adequate attention.

In recent years, musculoskeletal modeling and finite element analysis (FEA), have evolved as important tools in lower limb motion biomechanics research, and have been widely used in sports injury prediction, sports performance optimization and rehabilitation [11], [13]. FEA and OpenSim are both vital tools used in the study of lower limb biomechanics. FEA divides the lower limb's bone, muscle, and joint structures into multiple small elements through numerical simulations, enabling accurate analysis of stress distribution during movement. This helps in evaluating sports injuries, optimizing athletic posture, and designing artificial joints. FEA is widely used in sports injury prediction, rehabilitation and prosthesis design [24], [71], [73]. Previous studies employing FEA have examined factors such as joint stress distribution at different contact angles during running, as well as stress response patterns in individuals with lateral ankle ligament injuries [71], [77], [80]. Previous studies have employed recumbent Magnetic Resonance Imaging (MRI) for joint imaging and structural analysis of subjects [5], [8]. While recumbent MRI is typically used for static structural analysis, its inability to fully simulate dynamic motion has limited the comprehensive study of dynamic processes. In contrast, multi-position Helium-free Magnetic Resonance Imaging (MRI) technology allows for joint scanning in an upright position, enabling the capture of the position and shape of soft tissues such as joints and ligaments under the subject's own weight [2]. Moreover, Helium-free MRI utilizes a superconducting magnet system that does not rely on liquid helium cooling, significantly reducing both equipment costs and maintenance complexity, while offering enhanced image resolution and shorter scan times. OpenSim is a simulation tool that models the interactions between muscles, bones and joints, facilitating the analysis of mechanical changes across different movement patterns. It plays a pivotal role, particularly in gait analysis, musculoskeletal dynamics and rehabilitation training [56], [75]. Some studies have used the OpenSim model to simulate the effect of limited ankle dorsiflexion motion on starting and stopping movements, and the results demonstrate that knee stability is enhanced when the ankle dorsiflexion angle is restricted [75]. However, there is a lack of systematic research on the impact of ankle dorsiflexion motion during the CMJ process, particularly regarding its influence on knee injury risk.

This study aimed to combine musculoskeletal modeling and finite element analysis of the lower extremities to simulate the effects of varying ankle dorsiflexion movements on the biomechanical characteristics during the CMJ landing. The goal was to clarify the specific manifestations and patterns of knee injury risk under different ankle dorsiflexion conditions. The study hypothesizes that during the landing phase, a reduced ankle dorsiflexion ROM leads to increased knee joint stress and a higher risk of injury, with the knee joint exhibiting adaptive changes to compensate for the restricted dorsiflexion range.

2. Materials and methods

2.1. Study participant details

The sample size for this study was calculated using G*Power software (version 3.1.9.7; Heinrich Heine University Düsseldorf, Düsseldorf, Germany), based on effect sizes reported in previous studies examining biomechanical differences in lower limb movements between individuals with and without ankle dorsiflexion limitations. The analysis aimed to ensure sufficient statistical power (≥ 0.8) to detect significant differences in joint angle, torque, and muscle activation patterns during the CMJ landing, with the alpha level set at 0.05. Power analysis indicated that a minimum sample size of 25 participants would be adequate [55]. To account for potential dropouts and to enhance the robustness of the analyses, 32 male basketball players were recruited for this trial. Inclusion criteria were as follows: (1) participants aged 18–30 years, (2) regular engagement in basketball training, characterized by a minimum of three sessions per week, each lasting at least two hours, (3) no history of lower limb surgery or significant musculoskeletal injury in the past 6 months, (4) no underlying neurological or systemic conditions that might affect motor function.

To assess whether participants had limited ankle dorsiflexion, the Weight-Bearing Lunge Test (WBLT) was employed [25], [54]. The WBLT is a reliable and commonly used clinical assessment evaluating ankle dorsiflexion ROM in a functional, weight-bearing position. During the test, participants were instructed to keep their heel grounded and their feet flat on the floor, performing a lunge by advancing the knee towards a wall while maintaining heel contact with the ground. The participant was then asked to slowly bend the front knee and lunge forward as far as possible, aiming to bring the knee as close to or in contact with the wall without lifting the heel. Ankle flexibility was assessed by measuring the dorsiflexion angle using a protractor. The test was terminated if the heel was raised off the ground. The maximum dorsiflexion angle achieved while maintaining heel contact with the ground was recorded to accurately reflect the ankle joint's ROM. Three trials were conducted, and the average value was used for analysis.

Following the WBLT screening, participants were divided into two groups: the normal dorsiflexion (ND) group (n = 17, height: 184.6 ± 3.5 cm, age: 21.3 ± 1.5 years, weight: 75.4 ± 2.6 kg) and the limited dorsiflexion (LD) group (n = 15, height: 183.2 ± 2.8 cm; age: 22.1 ± 1.8 years, weight: 76.4 ± 3.1 kg). The use of the WBLT provided a functional assessment of ankle mobility, ensuring that the classification accurately reflected participants' ability to dorsiflex during weight-bearing activities. The comparison of average dorsiflexion amplitude of ankle joint between the normal dorsiflexion group and the limited dorsiflexion group is shown in Table 1. Prior to data collection, all participants were thoroughly briefed on the study's objectives, procedures, conditions and requirements. This ensured a more precise investigation of how limitations in dorsiflexion could influence lower limb biomechanics during dynamic movements, such as CMJ landing. Comprehensive details regarding the study were outlined in the consent form, and the study protocol was approved by the Ethics Committee of Ningbo University (Protocol code: TY2024031).

Table 1. Comparison of mean ankle dorsiflexion range between normal dorsiflexion group and limited dorsiflexion group

	ND (n = 17) Mean ± SD	LD (n = 15) Mean ± SD	P
Ankle dorsiflexion range in dominant leg [°]	40.2 ± 3.1	34.1 ± 2.9	0.032*
Ankle dorsiflexion range in the nondominant leg [°]	39.5 ± 2.4	34.3 ± 2.7	0.044*

* indicates a significant difference in ankle dorsiflexion ROM between the two groups ($p < 0.05$).

2.2. Biomechanics parameters collection and processing

In this study, participants were instructed to wear exercise tights and were fitted with reflective markers according to the Gait2392 musculoskeletal model, which features 23 joint degrees of freedom and 92 muscle-tendon actuators within the OpenSim framework (Fig. 1A). Electromyographic (EMG) signals were recorded from the target muscles using an EMG testing system (Fig. 1B). Motion trajectories were captured using the Vicon 3D motion capture system (Vicon Metrics, Ltd., Oxford, UK), while ground reaction forces were measured with an AMTI force platform (AMTI, Watertown, MA, USA). Kinematic and kinetic data were acquired at sampling frequencies of 200 Hz and 1000 Hz, respectively [65], [66]. EMG signals were recorded at 1000 Hz using the Delsys EMG system (Delsys, Boston, Massachusetts, USA) [66]. Before the start of the formal experiment, the calibration of the experimental equipment should be carried out first, and the stray points outside the experimental environment should be deleted in the Vicon system to avoid affecting the experimental environment. Then, the calibration rod with reflective marks should be held around the force table to ensure the normal operation of the camera and the normal acquisition of all reflection points. After that, the calibration rod is placed on the corner of the force measuring table to establish a spatial coordinate system. After the coordinate system is established, it is determined whether there is a hybrid force on the force measuring table. If there is a hybrid force, it needs to be eliminated manually. After the environmental calibration of the experimental equipment, static and dynamic test collection is carried out.

To ensure optimal performance and minimize the risk of injury, participants completed a 10-minute warm-up (including jogging, jumping, and stretching) at an

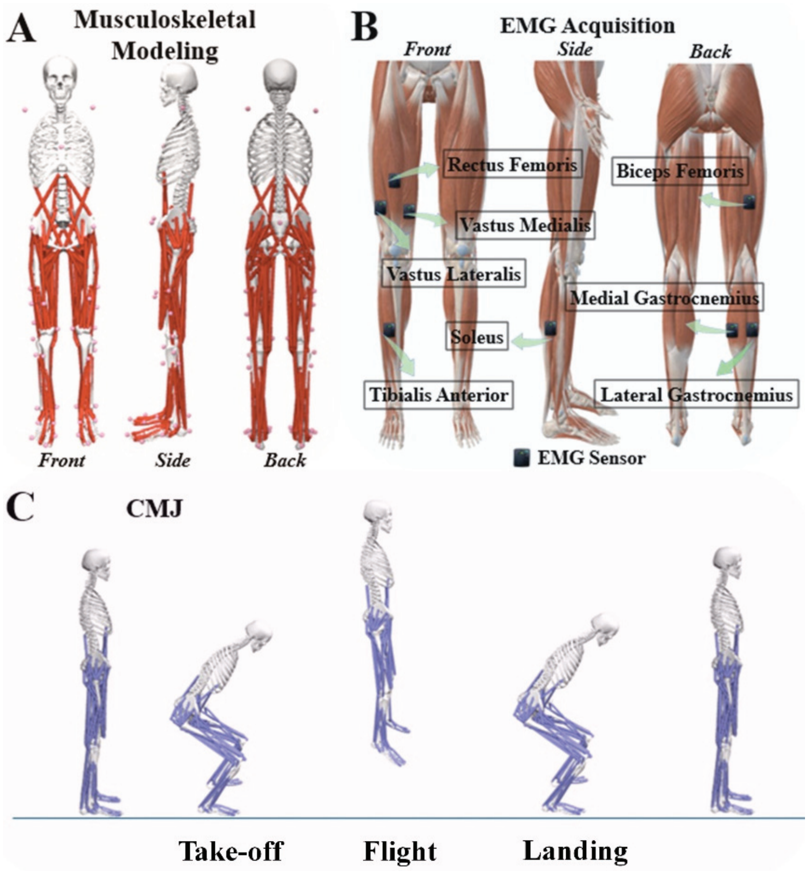

Fig. 1. (A) Schematic representation of marker points in the OpenSim musculoskeletal model, (B) schematic representation of EMG test locations, (C) schematic representation of CMJ test

adaptive intensity before the test. During the CMJ test (Fig. 1C), participants started hip-width apart and slightly rotated to provide stable support. They then crouched to stretch the lower limb muscle groups and connective tissues, with the arms positioned behind the body in preparation for the swing. Subsequently, participants swung their arms forward vigorously, extended their hips and jumped upwards as quickly as possible, maintaining a straight posture to achieve maximum height [43]. Upon landing, the front foot contacted the ground first, followed by the heel, and participants returned to a standing position. The study conducted a repeat test for each participant, in which each participant performed six jumps with a one-minute rest period between each jump, to prevent fatigue-related injuries and ensure the accuracy of the experimental data. Participants were instructed to exert 100 percent effort during each takeoff and to stabilize their bodies as much as possible during the landing. A sliding or unstable landing is recorded as a failure [78].

The landing phase was defined as the period from initial contact, when the ground reaction force exceeded 10 N, to maximum knee flexion [47]. Data on motion trajectories and ground reaction forces, simultaneously recorded by the Vicon motion capture system and AMTI force platform, were imported into MATLAB (Matlab R2022a, MASS, Natick, MA, USA) for analysis. The kinematic and kinetic data, originally in (.c3d) format, were transformed into (.trc) and (.mot) formats for further analysis in OpenSim. To enhance the accuracy of the model, the marker weights were adjusted based on the subjects' anthropometric parameters, ensuring that the subject-specific model aligned with the 2392 model when both were loaded. Joint angles were computed using inverse kinematics, while joint moments were determined through inverse kinetics [31]. Static optimization algorithm was employed to estimate muscle activation and muscle forces. The raw EMG signals were first filtered using a fourth-order Butterworth bandpass filter (10–500 Hz) in the Delsys EMG analysis software, after which the root mean square (RMS) values were calculated. To normalize the EMG amplitudes, they were expressed as a percentage of the maximal voluntary isometric contraction (MVIC) for each muscle. Muscle activation levels were quantified on a scale from 0 (no activation) to 1 (full activation) by dividing the RMS amplitude during the test by the RMS amplitude from the MVIC. The muscle activation data

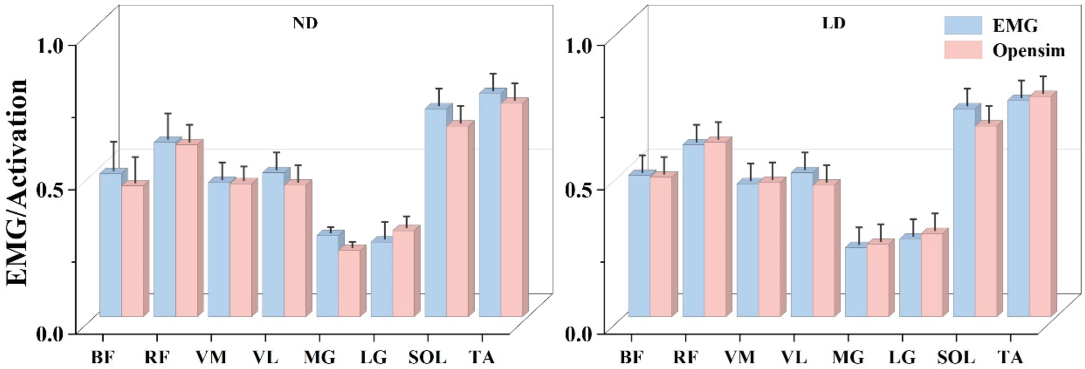

Fig. 2. Schematic representation of EMG muscle activation with blue areas representing EMG muscle activation results and red areas representing muscle activation results from the musculoskeletal model. The vertical scale ranges from 0 to 1, indicating the level of muscle activation from none to full activation

obtained from the EMG sensors were compared with the musculoskeletal model simulation results to evaluate the model's accuracy and validity. No significant differences were found between the activation levels from the EMG data and those from the musculoskeletal model simulations (Fig. 2).

The coactivation of muscles surrounding the knee joint during the landing phase of the CMJ was determined using Eq. (1) [44]:

$$Muscleco-activation\ (\%) = \left(\frac{RMSEMG_{antaonist}}{RMSEMG_{agonist}}\right)\times 100. \tag{1}$$

During the CMJ landing phase, the patellofemoral joint contact force (PTF) is determined using Eq. (2), where (x) represents the knee flexion angle, (Mk) represents the knee extensor moment [28]. The knee flexion angle was determined using the nonlinear equation for the quadriceps lever arm, as described below [34]:

$$Lq = 0.00008x^3 - 0.013x^2 + 0.28x + 0.046\,. \tag{2}$$

The strength of the quadriceps (Fq) refers to quadriceps strength:

$$Fq = \frac{Mk}{Lq}\,. \tag{3}$$

The constant k is the constant that correlates with the knee angle position [60]:

$$K = \frac{0.462 + 0.00147x^2 - 0.0000384x^2}{(1 - 0.0162x^2 + 0.000155x^2 - 0.000000698x^3)}\,. \tag{4}$$

The PTF was calculated based on the quadriceps force (Fq) and a constant k:

$$PTF = Fq \times k\,. \tag{5}$$

2.3. Quantification and statistical analysis

This study examined changes in lower limb biomechanics during the landing phase of the CMJ. The biomechanical data were normalized to 101 data points, representing the full range from 0 to 100% of the landing phase. All variables in this study are normally distributed after Shapiro–Wilk test. To assess differences in joint kinematics and kinetics between the two groups, independent sample t-tests were conducted, with statistical analysis performed using SPSS 27. The significance level was set at $p < 0.05$. Lastly, the data were imported into Origin 2022 software for graphical representation and visualization.

2.4. Finite element analysis of foot–knee integration model

2.4.1. Model construction

Two healthy male subjects, with no history of ankle and knee pain or lower extremity surgery, underwent magnetic resonance imaging (Helium-free MRI) and computed tomography (CT) scans to assess those with high and low ankle dorsiflexion ROM, respectively. While standing, the knee joint was fully extended, and the ankle joint was positioned in a neutral alignment. The knee joint was subsequently scanned using a Helium-free MRI system (Fig. 3A). The repetition time and echo time were set to 500 ms and 14 ms, respectively, with a 20 cm field of view and a slice thickness of 1 mm. During the MRI image processing and model creation, the images were imported into Mimics 21.0 (Materialise, Leuven, Belgium), where bone and soft tissue boundaries were identified and segmented using gray value determination and region-based segmentation techniques. These were then exported in STL file format. The bone, ligaments, and skin were imported into Geomagic Studio 2021 (Geomagic, Inc., Research Triangle Park, NC, USA) for noise reduction, smoothing, surface creation, and fitting, and subsequently exported in IGES format. Each component was converted into a solid using SolidWorks 2022 (SolidWorks Corporation, Waltham, MA, USA), and the joint position was assembled based on orthogonal plane projections of the subject's knee joint during landing, ensuring consistency with the actual X-ray images. The model was subsequently constructed in Workbench 2021 (ANSYS, Inc., Canonsburg, PA, USA), where contact conditions were specified, and the tetrahedral mesh was employed for model discretization (Fig. 3B). After performing a mesh convergence test, the bone mesh was set to a size of 2.0 mm, while the mesh size for the anterior cruciate ligament (ACL) and posterior cruciate ligament (PCL) was reduced to 0.5 mm. The meniscus, ligaments, and cartilage were assigned to a mesh size of 1.0 mm.

2.4.2. Material properties, boundaries and loading conditions

All materials, except for the encapsulated soft tissue, ACL and PCL, were modeled as linear elastic, with their elasticity characterized by Young's modulus (E) and Poisson's ratio (v). The soft tissue, ACL and PCL were treated as hyperelastic materials, represented using the Mooney–Rivlin model. The material properties for each component are provided in Table 2.

Building on this foundation, the model was locally refined according to the geometric features of the contact areas. A contact group was subsequently created to define the bonding relationships between the cartilage and bone, as well as between the origins of each ligament and bone, and the meniscus and bone. To model the sliding friction between the meniscus and femoral cartilage, as well as between the patellar and femoral cartilage, a friction coefficient of 0.04 was applied [23], [26]. Frictionless contact between cartilage and the bone surface and between the ACL and PCL was defined based on previous indications [4]. The anchor points of bone and cartilage are encapsulated soft tissues. For the foot-knee model placement, the knee joint was preset to a neutral position. The knee joint angle was determined by adjusting the an-

Table 2. Material parameters for each structure

Component	Elastic modulus [MPa], E	Poisson's ratio: v	Destiny [kg/m³]	Ref.
Skin	Hyperelastic (first-order Ogden model, $\mu = 0.122$ kPa, $\alpha = 18$)	N/A	950	[50]
Bulk soft tissue	Hyperelastic (secondorder polynomial strain, $C_{10} = 0.8556$, $C_{01} = 0.05841$, $C_{20} = 0.03900$, $C_{11} = 0.02319$, $C_{02} = 0.00851$, $D_1 = 3.65273$)	N/A	950	[24]
Aterior Crucial Ligament	Hyperelastic (first-order polynomial strain, $C_1 = 1.95$, $D = 0.00683$)	N/A	1000	[51]
Posterior Crucial Ligament	Hyperelastic (first-order polynomial strain, $C_1 = 3.25$, $D = 0.0041$)	N/A	1000	[51]
Fibula, Tibia, Femur, and Patella	14220	0.3	1990	[27]
Foot Bones	7300	0.3	1500	[12]
Knee Cartilages	20	0.46	1000	[38]
Foot Cartilages	1	0.4	1050	[57]
Medial and Lateral Collateral Ligament	467	0.46	1000	[20]
Medial and Lateral Meniscus	59	0.49	2000	[37]
Patellar Tendon	778	0.46	1000	[3]
Foot Ligaments	260	0.4	1000	[57]
Plantar Fascia	350	0.4	1000	[9]
Patellar Tendon	816	0.3	1000	[10]
Plate	17000	0.4	1000	[79]

gle between the femoral axis, tibial axis and the longitudinal axis of the foot in the sagittal plane [23]. A fixed ground plate and femoral interface were used for the analysis, with a contact surface featuring a friction coefficient of 0.6 to model the foot-ground interaction, while the femoral interface remained stationary (Fig. 3D) [68]. The peak ground reaction force during CMJ landing, along with the corresponding kinematic, kinetic, and muscle force data used for the finite element (FE) analysis, are presented in Table 3.

Table 3. Finite element model of the knee joint with applied loads

Experimental variables		ND	LD
Ground Reaction Force [N]	Posterior	254.15	251.40
	Medial	231.16	226.34
	Vertical	1562.22	1801.27
Ankle Angle [°]	Dorsiflexion	24.18	26.24
Knee Angle [°]	Flexion	94.35	89.85
	Adduction	1.44	1.31
	Ext Rot	10.10	13.07
Muscle Force [N]	Biceps Femoris	360.77	348.23
	Rectus Femoris	974.89	1116.03
	Vastus Medialis	196.56	150.43
	Vastus Lateralis	356.18	324.48
	Medial Gastrocnemius	499.91	661.37
	Lateral Gastrocnemius	180.69	146.42
	Soleus	378.30	370.70
	Tibialis Anterior	684.71	671.56

2.4.3. Model validation

In this study, the finite element model was validated through both axial stress and anterior drawer experiments [18], [58], [59]. A 134 N forward thrust was applied to the upper end of the tibia, displacing the midpoint of the tibial intercondylar ridge, like the force used in the anterior drawer test of the knee. Previous studies have reported anterior displacements of 4.0, 4.3, 4.13 and 4.18 mm, which are in good agreement with the simulation result of 4.15 mm obtained in this study, thus confirming the validity of the finite element model [18], [59], [68]. Furthermore, a high-speed double-perspective imaging system (DFIS) (Fig. 3F) was employed to capture fluoroscopic images of the subject's knee joint during landing. The DFIS parameters were set as follows: source image distance of 1350 mm, device voltage at 60 kV, device current of 500 mA, exposure time of 3 seconds, laser wavelength of 650 nm, and an automatic exposure control dose range of 45 μGy. The flat panel detector had a resolution of 3072 × 3072 pixels, with an X-ray area of 427 × 427 mm. The X-ray tube operated at a nominal voltage of 150 kV, the laser power was 3 mW, and the angle sector was 90°. The knee joint displacement results obtained from fluoroscopic imaging were compared with the FEA results to further validate the finite element model (FEM) [15], [32], [39]. DFIS captured X-ray information and generated reliable gray-scale medical images after processing the data using different attenuation levels in various tissues and organs (Fig. 3F). The Vicon motion capture system and force platform were used to synchronize the kinematic and kinetic data, which were subsequently inputted into the finite element model (Fig. 3C). The knee joint image acquired by the fluoroscopy system through two orthogonal planar projections, and the knee joint model was calibrated and aligned using 3D modeling software to ensure consistency with the actual X-ray image (Figs. 3G, H). The knee joint displacement accurately calculated using the coordinate system calculator plugin in Rhinoceros software (Fig. 3I) [32], [39]. The results demonstrate that the knee displacement calculations derived from finite element analysis and DFIS show strong consistency in 3D space, validating the feasibility and reliability of the constructed finite element model (Fig. 3J).

3. Results

3.1. Kinematics and kinetics

As shown in Fig. 4, the differences in kinematics and kinetics and the peak kinematics and kinetics between ND and LD during the landing phase of the CMJ. In terms of ankle differences, the dorsiflexion Angle of ND was higher than that of LD during the 4–38% stage ($p < 0.001$), and the ankle moment was higher than that of LD during the whole stage of landing ($p = 0.001$). In terms of peak results, the peak plantar flexion moment of the ankle joint was lower in ND than in LD ($p < 0.001$).

In terms of knee joint differences, the knee extension moment of ND was greater than that of LD at the 0–7% stage ($p = 0.032$) and was smaller than that of LD at the 8–20% stage ($p = 0.021$). The knee abduction Angle was smaller than that of LD at the 5–50% stage and 70–90% stage ($p = 0.003$, $p = 0.001$, respectively). The knee abduction moment was lower than LD at 19–70% stage ($p < 0.001$), and the knee external rotation Angle was lower than LD at 0–18% stage and 24–67% stage ($p = 0.009$, $p < 0.001$, respectively). The knee external rotation torque was less than LD at 10–18% stage and 43–100% stage ($p = 0.043$, $p = 0.001$, respectively). In terms of peak results, ND had higher knee flexion moments ($p = 0.02$), lower abduction and adduction angles ($p = 0.04$, $p = 0.005$,

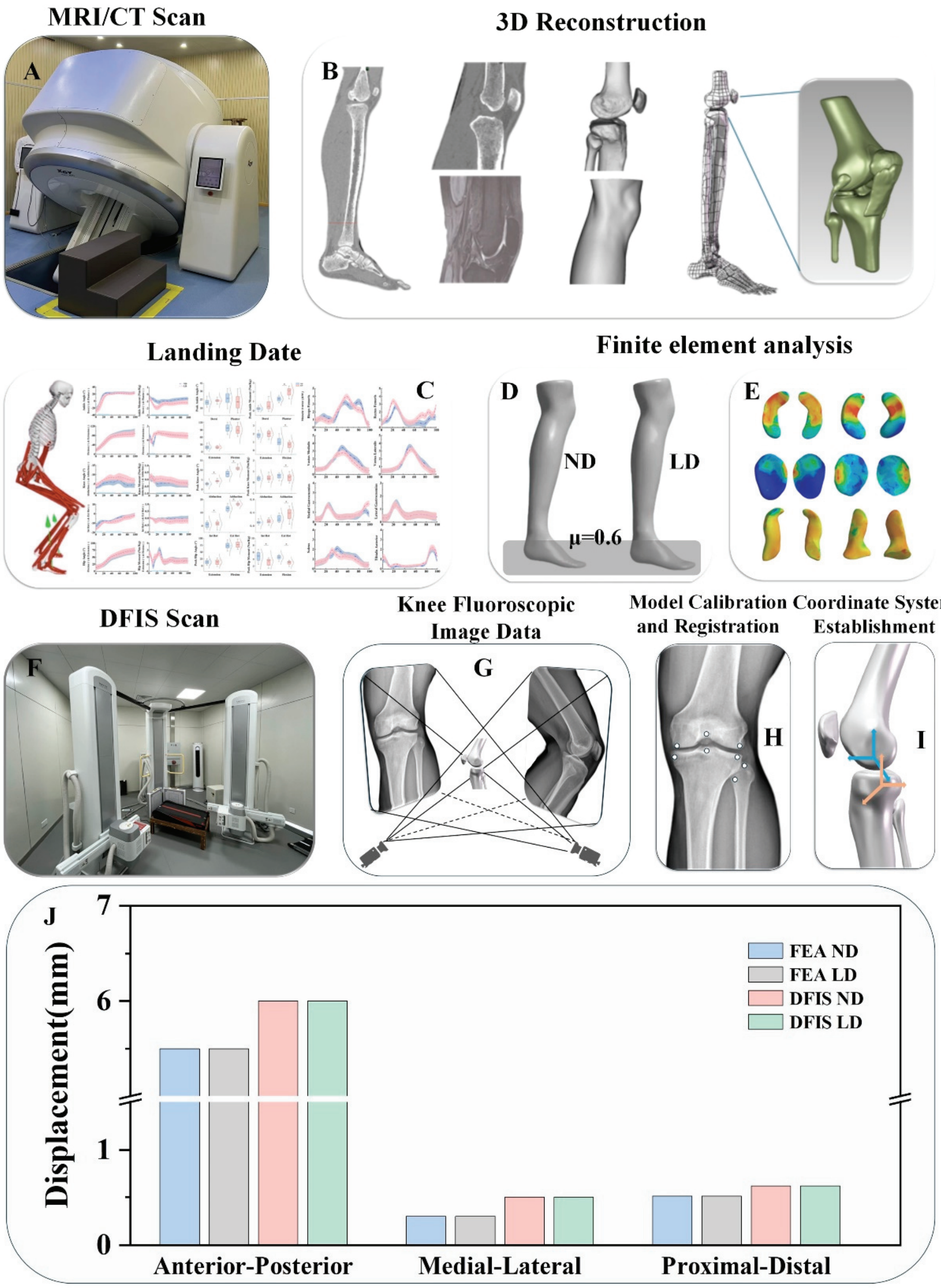

Fig. 3. Illustration of the finite element model establishment and validation process:
(A) foot and knee data were obtained using CT and MRI scanning techniques,
(B) creation of a finite element model of the knee joint, including the configuration of muscles, bones, and ligaments,
(C)–(E) import biomechanical data into the finite element model for simulation and visualization of the results,
(F)–(G) data acquisition and processing of knee joint fluoroscopy images acquired by DFIS, establishment and registration of (H)–(I) coordinate system, (J) comparison of knee displacement calculated based on DFIS and finite element analysis

respectively), higher adduction moments ($p = 0.026$), and lower external rotation and internal rotation angles than LD ($p = 0.038$, $p = 0.005$, respectively). The external rotation torque was less than LD ($p = 0.02$).

In terms of the difference in the hip joint, ND had a higher hip flexion moment than LD in the 7–17% stage ($p = 0.006$) and lower than LD in the 21–37% stage ($p = 0.01$). In terms of peak results, ND had

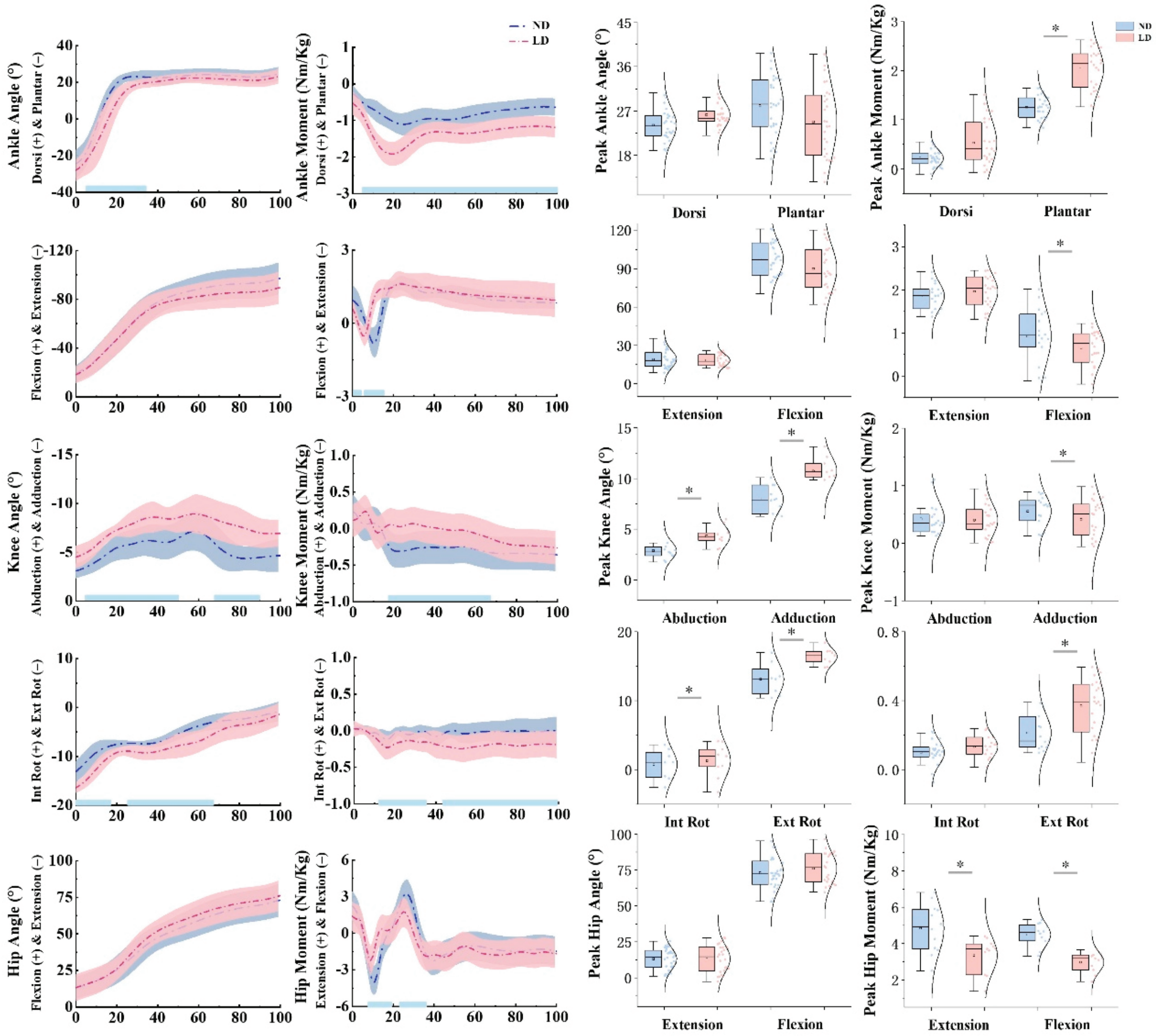

Fig. 4. Illustration of the kinematic and kinetic differences between ND and LD during CMJ testing. Blue lines and "*" indicate significant differences ($p < 0.05$)

higher hip extension moment and flexion moment than LD ($p = 0.006$, $p < 0.001$, respectively).

3.2. Muscle activation and muscle force

As shown in Fig. 5, the differences in muscle activation and muscle force between ND and LD during the landing phase of the CMJ. In terms of muscle activation, the rectus femoris activation degree of ND was higher than that of LD at 21–46% stage ($p < 0.001$) and was lower than that of LD at 72–91% stage ($p = 0.001$). The vastus medialis activation degree was higher than that of LD at 63–83% stage ($p = 0.001$). The activation degree of the vastus lateralis muscle was higher than that of LD at stage 63–87% ($p = 0.001$), and the activation degree of soleus muscle was higher than that of LD at 17–35% stage ($p < 0.001$), and lower than that of LD at 38–49% stage ($p = 0.027$). The activation of the tibialis anterior muscle was less than that of LD at 17–22% and 82–96% stages ($p = 0.041$, $p = 0.001$, respectively).

In terms of muscle strength, the biceps femoris muscle strength of ND was lower than that of LD at 48–68% stage ($p = 0.001$) and 38–49% stage ($p < 0.001$), and the rectus femoris muscle strength was lower than that of LD at 9–30% stage and 63–100% stage ($p = 0.013$, $p < 0.001$, respectively). The muscle strength of the vastus medialis was higher than that of LD at 62–83% stage ($p = 0.001$), the muscle strength of the vastus lateralis was higher than that of LD at 65–86% stage ($p = 0.001$), and the muscle strength of the medial gastrocnemius was lower than that of LD

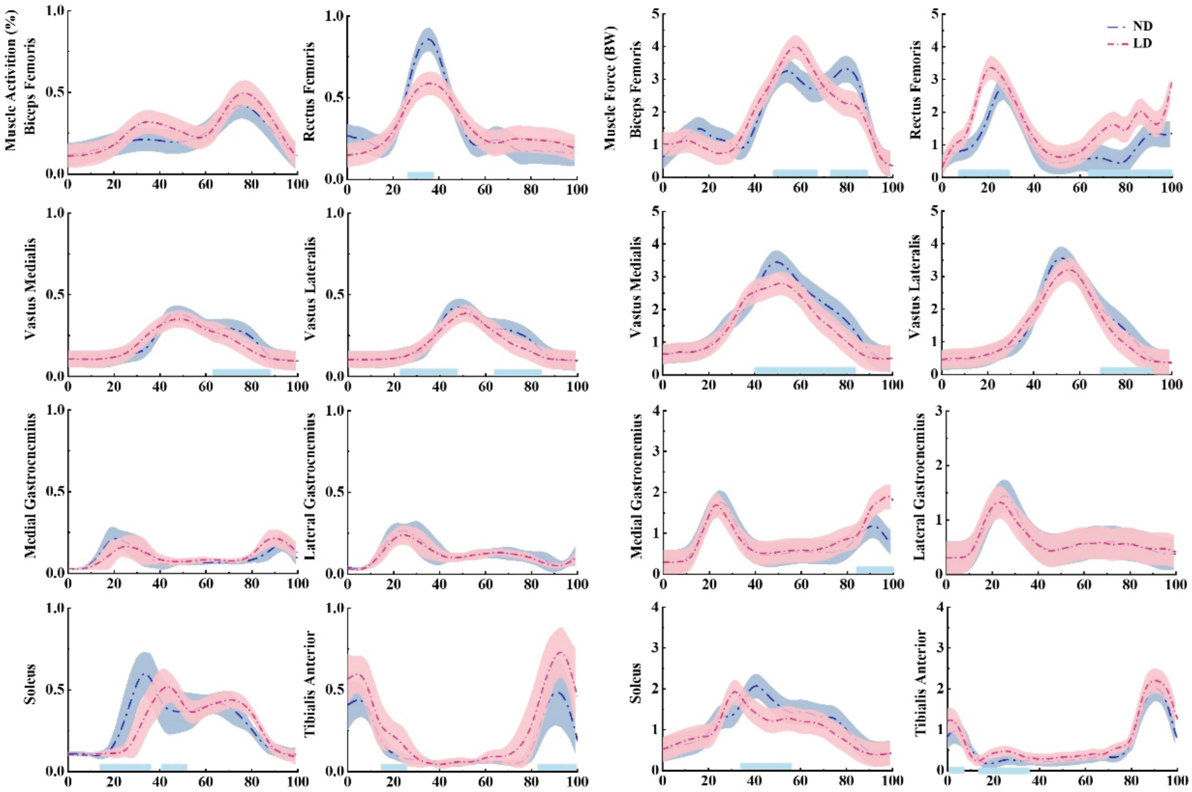

Fig. 5. Illustration of the muscle activation and muscle force differences between ND and LD during CMJ testing. Blue lines and "*" indicate significant differences ($p < 0.05$)

at 83–100% stage ($p = 0.001$). Soleus muscle strength was higher than LD at 34–56% stage ($p = 0.023$), and the tibialis anterior muscle strength was higher than LD at 0–8% stage and 14–31% stage ($p = 0.031$, $p = 0.009$, respectively).

3.3. Joint contact force and muscle coactivation

As shown in Fig. 6, the differences in knee contact force, patellar joint contact force, and degree of muscle coactivation around the knee between ND and LD during the landing phase of the CMJ. In the sagittal plane, the knee contact force of ND was lower than that of LD in the 15–38% stage ($p = 0.034$). In the coronal plane, the knee contact force of ND was higher than that of LD in the 10–15% stage ($p = 0.028$) and lower than that of LD in the 21–30% stage ($p = 0.024$). The knee contact force in the horizontal plane was lower than that in the LD at 10–20% stage ($p = 0.028$). The contact force of ND was higher than that of LD at the stage of 8–20% ($p < 0.001$). In terms of muscle coactivation, BF/RF, BF/VF, TA/SOL, and TA/GM of

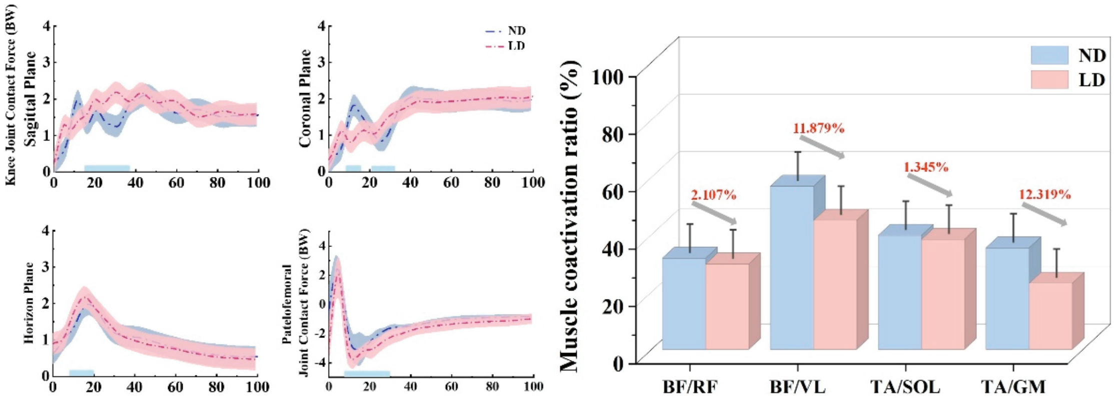

Fig. 6. Illustration of the knee contact force, patellar joint contact force, and muscle coactivation differences between ND and LD in the CMJ test. Blue lines and "*" indicate significant differences ($p < 0.05$)

ND were by 2.107, 11.879, 11.345 and 12.319% higher than those of LD, respectively.

3.4. Finite element analysis

In Figure 7, the differences between ND and LD in the von Mises stress distributions such as ligaments and soft tissues during the landing phase of the CMJ are outlined. The average von Mises stress and the peak von Mises stress of the medial tibial cartilage in ND were 2.492 and 4.896 MPa, respectively. The average von Mises stress and the peak von Mises stress of the medial tibial cartilage in LD were 4.558 and 8.541 MPa. The average von Mises stress and the peak von Mises stress in the lateral tibial cartilage of ND were 2.296 and 4.519 MPa, respectively. The average von Mises stress and the peak von Mises stress in the medial tibial cartilage of LD were 4.214 and 8.125 MPa, respectively. The average von Mises stress and the peak von Mises stress of the posterior cruciate ligament in ND was 10.665 and 21.159 MPa, respectively. The average von Mises stress and the peak von Mises stress of the posterior cruciate ligament in LD was 14.161 and 27.846 MPa. The mean von Mises stress and the peak von Mises stress of the ACL in ND were 8.445 and 16.685 MPa, respectively. The mean von Mises stress and the peak von Mises stress of the ACL in LD were 12.027 and 23.754 MPa. The mean von Mises stress and the peak von Mises stress of the medial meniscus in ND were 8.353 and 16.624 MPa, respectively. The mean von Mises stress and the peak von Mises stress of the medial meniscus in LD was 10.224 and 20.259 MPa. The mean von Mises stress and the peak von Mises stress of the lateral meniscus in ND were 7.935 and 15.793 MPa, respectively. The mean von Mises stress and the peak von Mises stress of the lateral meniscus in LD were 9.712 and 19.246 MPa.

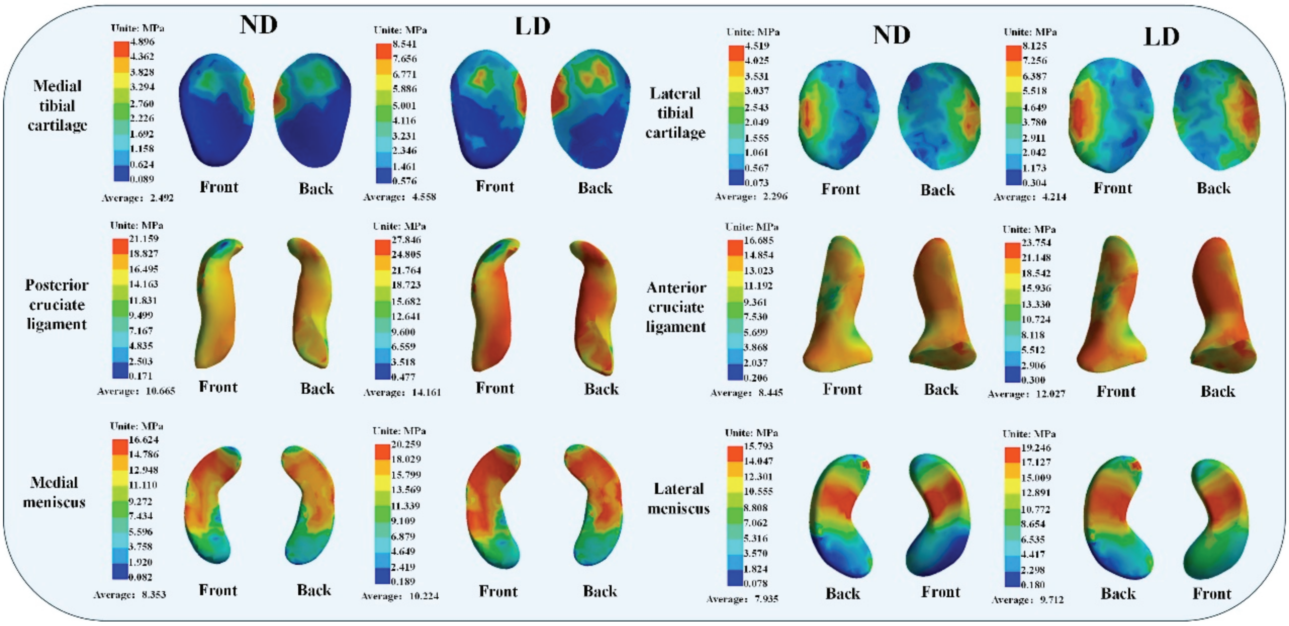

Fig. 7. Visualization of the von Mises stress distribution of the tibial cartilage, cruciate ligaments, and menisci during the landing phase of the CMJ test for ND and LD

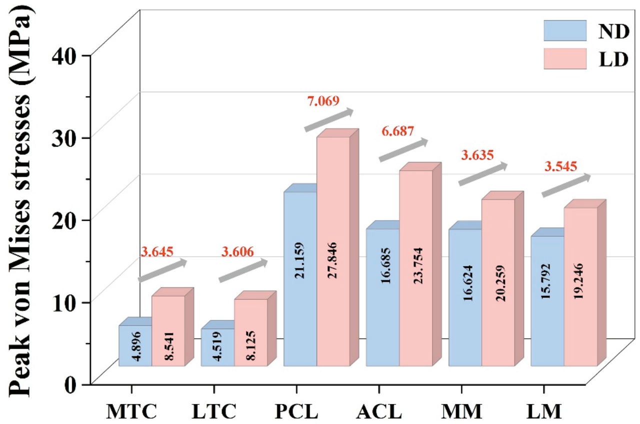

Fig. 8. Visualization of von Mises peak stress changes in the tibial cartilage, cruciate ligaments, and menisci during the landing phase of the CMJ test for ND and LD

As shown in Fig. 8, the differences in peak von Mises stress changes such as ligaments and soft tissues between ND and LD during the landing phase of the

CMJ were observed. Compared with ND, LD increased 3.645 MPa in the medial tibial cartilage, 3.606 MPa in the lateral tibial cartilage, 7.069 MPa in the posterior cruciate ligament, 6.687 MPa in the anterior cruciate ligament, 3.635 MPa in the medial meniscus, and 3.545 MPa in the lateral meniscus.

4. Discussion

The authors of this study investigated how varying levels of ankle dorsiflexion affect lower limb biomechanics during the cushion-landing phase. We hypothesized that a reduced ankle dorsiflexion ROM during landing would increase knee joint stress, thereby heightening the risk of injury. Additionally, we anticipated that the knee joint would exhibit adaptive changes to compensate for the limited ankle dorsiflexion. The results of this study supported the initial hypothesis and revealed several key findings: (1) with a lower ankle dorsiflexion ROM, the knee joint demonstrated increased adduction, and external rotation angles during the landing buffer phase, accompanied by higher von Mises stresses in the tibial cartilage, meniscus, ACL and PCL; (2) a reduced ankle dorsiflexion ROM was associated with smaller contact forces of the patella and knee joint in the horizontal plane; (3) at lower dorsiflexion ROM, muscle activation of the rectus femoris, vastus medialis, and vastus lateralis was lower at certain stages, while the activation of the soleus occurred later in the movement; (4) the muscle coactivation around the knee joint (BF/RF, BF/VL, TA/SOL, TA/GM) was reduced when the ankle joint ROM was limited.

During the CMJ landing, subjects typically transitioned from plantar flexion to dorsiflexion of the ankle joint. The findings of this study showed that the ND group displayed a greater ankle dorsiflexion angle than the LD group, whereas the LD group exhibited a higher peak plantar flexion moment. These results align with previous research, which has proposed that greater ankle plantarflexion may increase the ankle's ROM, thus enhancing its capacity to absorb impact forces and potentially lowering the risk of knee injuries [17], [36], [68]. Additionally, the LD group displayed greater knee adduction and external rotation angles, as well as higher joint forces during landing. The knee joint is essential for maintaining balance during dynamic movements [62], with the contact force between the patella and femur being a key factor in knee stability. In this study, the patellar joint contact force (PTF) was calculated using a specific formula [28], [34], [60], and the results indicated that, compared to the LD group, the ND group exhibited higher patellar joint contact forces at certain stages of the landing phase. This phenomenon is likely attributable to the larger dorsiflexion ROM in the ND group. A greater dorsiflexion angle facilitates a larger range of ankle motion, which may enable the lower limbs to absorb more of the impact forces during landing [17], [29]. Previous research has also shown that a limited dynamic functional ROM in the ankle joint is associated with a higher risk of injury during jumping and landing activities [69]. For example, healthy female athletes typically demonstrate a larger dynamic functional range during landing, and modifying the initial contact angle of the ankle joint can effectively lower the risk of knee injuries [42], [62].

In terms of muscle activation, the results of this study indicate that the LD group exhibited lower muscle activation of the rectus femoris, vastus medialis, and vastus lateralis at certain stages compared to the ND group, with delayed activation of the soleus. Additionally, muscle coactivation around the knee joint (BF/RF, BF/VL, TA/SOL, TA/GM) was lower in the LD group when ankle joint motion was limited. Previous research on the effects of physical therapy for patellar tendinopathy has shown that increasing ankle dorsiflexion through rehabilitation can improve knee function, reduce pain and enhance lower limb strength and stability in patients with patellar tendinopathy [14]. The findings of the present study suggest that greater ankle motion may contribute to enhanced knee stability and muscle control. Although no significant changes were observed in knee flexion angles, adaptive coactivation of the muscles was noted, suggesting that ankle motion may contribute to knee stability. The muscle adaptations could enhance the peripatellar muscles' ability to withstand higher loads, potentially through hypertrophy or improved efficiency in absorbing impact forces. Previous studies have highlighted the importance of coactivation patterns among the muscles surrounding the knee in maintaining dynamic knee stability and preventing injuries [19], [30]. Muscle coactivation is crucial for converting valgus forces into joint contact forces, thus protecting the knee from injury [53], [63].

In this study, participants' lower limbs were scanned using Helium-free MRI and CT. Compared to traditional MRI, Helium-free MRI employs a cooling system with zero or very low volatilization, reducing reliance on expensive and unstable liquid helium, and offering a more environmentally friendly alternative [2]. Its innovative magnet design supports multi-position imaging, including standing, sitting, prone, and lateral lying positions, better aligning with the natural posture and biomechanical characteristics of the human body. This makes it particularly suitable for examining the spine, joints and musculoskeletal system, allowing for the detection of issues that may not be observable in the supine position. Multi-position MRI enhances the accuracy of joint, ligament and tendon imaging, providing a more realistic simulation of tissue loading during physical activity. A finite element model of the foot and knee-integrated lower extremity was developed to more accurately simulate real-life conditions and calculate stress distribution in the knee joint and its surrounding structures [40]. The results indicated that, in the limited dorsiflexion (LD) condition, along with an increase in knee adduction and external rotation angles, there was a corresponding increase in knee adduction and external rotation torques, as well as a decrease in patellar joint contact forces at certain stages. Additionally, the muscle coactivation around the knee joint was lower in the LD condition. The finite element analysis further revealed that LD was associated with higher stress in the tibial cartilage, meniscus, ACL and PCL compared to normal dorsiflexion (ND). This suggests that as the dorsiflexion motion of the ankle joint is reduced, the stress in these structures increases, resulting in greater impact loading on the knee joint, which, in turn, heightens the risk of injury [6], [7], [41]. Previous research has indicated that a reduced plantar flexion angle of the ankle during landing may elevate the risk of ACL injury [36], [67]. The present findings demonstrated that ACL stress was primarily concentrated in the attachment areas of the femur and tibia as well as in the medial and lateral regions. Notably, ACL tears are frequently observed in the femoral attachment area [22], [46]. In conclusion, the findings of this study indicate that restricted ankle dorsiflexion during landing results in heightened stress on the meniscus and femoral cartilage, which in turn increases the impact load on the knee joint and elevates the risk of knee injuries. These findings highlight the importance of modifying ankle joint motion, particularly increasing ankle dorsiflexion, to effectively reduce knee joint pressure and lower the likelihood of sports-related injuries.

The limitations of the present study must be acknowledged. First, the initial data collection through CT and MRI involved a cohort of male participants in good health. Due to inherent individual differences, the results of this study may not be universally applicable and could vary across different populations. Additionally, the simulation of the tibial ACL as a linear elastic material may have influenced the accuracy of the results for these ligaments. This simplification, however, is commonly used in prior research to improve computational efficiency. Furthermore, the study was conducted under controlled laboratory conditions, which may not fully reflect the conditions encountered in actual competitive settings. Future studies should aim to conduct experiments under conditions that more closely simulate real-world competitive environments to improve the external validity of the findings. Meanwhile this study included 32 male basketball players, the sample size – although likely sufficient for certain analyses – may still benefit from a larger and more diverse cohort, including different genders and athletes of varying competitive levels, to enhance the statistical power and generalizability of the results.

Future research can further optimize computational modeling and simulation to enhance the precision of personalized injury risk prediction and the realism of biomechanical simulations. First, a more refined foot-knee-hip integrated model can be developed to extend the current knee-focused analysis, enabling a comprehensive investigation of lower limb kinetic chains and the interplay between the hip, knee, and ankle injury mechanisms [67]. Second, machine learning and deep learning algorithms can be incorporated to optimize musculoskeletal modeling and FEA parameters, leveraging individualized biomechanical data to improve injury risk prediction and develop personalized intervention strategies [70]. Finally, wearable sensor technology (e.g., inertial measurement units and pressure insoles) can be employed to capture real-world biomechanical data during competitive play, facilitating validation of simulation models and enhancing their applicability and predictive accuracy in dynamic sports environments.

5. Conclusions

This study explored how different levels of ankle dorsiflexion affect knee joint impact load during landing, utilizing a personalized musculoskeletal model and a finite element model that integrates the foot and knee. The results indicate that greater ankle dorsiflexion during landing may effectively reduce internal tissue stress in the knee joint and enhance muscle coactivation around the knee, as well as increase the patellar joint contact force. These findings provide valuable theoretical support for strategies to reduce the risk of knee injuries during landing. Moreover, they offer reliable technical methods and theoretical references for the study of injury mechanisms in other athletic activities, such as running and lateral jumping.

Data availability

All data relevant to the current study are included in the article, further inquiries can be directed at the corresponding author.

Funding

This study was sponsored by the Ningbo key R&D Program (2022Z196), Research Academy of Medicine Combining Sports, Ningbo (No. 2023001), the Project of NINGBO Leading Medical & Health Discipline (No. 2022-F15, No. 2022-F22), Ningbo Natural Science Foundation (2022J065, 20221JCGY010607), Public Welfare Science & Technology Project of Ningbo, China (2023S145), and Zhejiang Rehabilitation Medical Association Scientific Research Special Fund (ZKKY2023001).

References

[1] BACKMAN L.J., DANIELSON P., *Low range of ankle dorsiflexion predisposes for patellar tendinopathy in junior elite basketball players: a 1-year prospective study*, The American Journal of Sports Medicine, 2011, 39 (12), 2626–2633, DOI: 10.1177/0363546511420552.

[2] BAGDINOVA A., RYBAKOV A., DEMIKHOV E., DEMIKHOV T., LYSENKO V., TARASOV V., SHUMM B., DMITRIEV D., *Simulation of a Gradient System for a Helium-Free Magnetic Resonance Imager*, Instruments and Experimental Techniques, 2022, 65 (1), 113–122, DOI: 10.1134/S0020441222010018.

[3] BALDWIN M.A., CLARY C.W., FITZPATRICK C.K., DEACY J.S., MALETSKY L.P., RULLKOETTER P.J., *Dynamic finite element knee simulation for evaluation of knee replacement mechanics*, Journal of Biomechanics, 2012, 45 (3), 474–483, DOI: 10.1016/j.jbiomech.2011.11.052.

[4] BENDJABALLAH M.Z., SHIRAZI-ADL A., ZUKOR D., *Biomechanics of the human knee joint in compression: reconstruction, mesh generation and finite element analysis*, The Knee, 1995, 2 (2), 69–79, DOI: 10.1016/0968-0160(95)00018-K.

[5] BENOS L., STANEV D., SPYROU L., MOUSTAKAS K., TSAOPOULOS D.E., *A review on finite element modeling and simulation of the anterior cruciate ligament reconstruction*, Frontiers in Bioengineering and Biotechnology, 2020, 8, 967, DOI: 10.3389/fbioe.2020.00967.

[6] BUCKWALTER J.A., *Sports, joint injury, and posttraumatic osteoarthritis*, Journal of Orthopaedic and Sports Physical Therapy, 2003, 33 (10), 578–588, DOI: 10.2519/jospt.2003.33.10.578.

[7] BUCKWALTER J.A., ANDERSON D.D., BROWN T.D., TOCHIGI Y., MARTIN J.A., *The roles of mechanical stresses in the pathogenesis of osteoarthritis: implications for treatment of joint injuries*, Cartilage, 2013, 4 (4), 286–294, DOI: 10.1177/1947603513495889.

[8] CHANDRAN A.S., TRIVEDI R., MODI B., PATEL R., *Estimation of stress and strain of knee joint using finite element analysis*, Journal of Physics: Conference Series, 2021, 012217, DOI: 10.1088/1742-6596/2070/1/012217.

[9] CHEN W.-M., LEE T., LEE P.V.-S., LEE J.W., LEE S.-J., *Effects of internal stress concentrations in plantar soft-tissue – a preliminary three-dimensional finite element analysis*, Medical Engineering and Physics, 2010, 32 (4), 324–331, DOI: 10.1016/j.medengphy.2010.01.001.

[10] CHEN W.-M., PARK J., PARK S.-B., SHIM V.P.-W., LEE T., *Role of gastrocnemius–soleus muscle in forefoot force transmission at heel rise – A 3D finite element analysis*, Journal of Biomechanics, 2012, 45 (10), 1783–1789, DOI: 10.1016/.jbiomech.2012.04.024.

[11] CHEUNG J.T.-M., ZHANG M., *A 3-dimensional finite element model of the human foot and ankle for insole design*, Archives of Physical Medicine and Rehabilitation, 2005, 86 (2), 353–358, DOI: 10.1016/j.apmr.2004.03.031.

[12] CHEUNG J.T.-M., ZHANG M., LEUNG A.K.-L., FAN Y.-B., *Three-dimensional finite element analysis of the foot during standing – a material sensitivity study*, Journal of Biomechanics, 2005, 38 (5), 1045–1054, DOI: 10.1016/j.jbiomech.2004.05.035.

[13] CHEUNG J.T.-M., YU J., WONG D.W.-C., ZHANG M., *Current methods in computer-aided engineering for footwear design*, Footwear Science, 2009, 1 (1), 31–46, DOI: 10.1080/19424280903002323.

[14] COELHO B.A.L., DAS NEVES RODRIGUES H.L., ALMEIDA G.P.L., JOÃO S.M.A., *Immediate effect of ankle mobilization on range of motion, dynamic knee valgus, and knee pain in women with patellofemoral pain and ankle dorsiflexion restriction: a randomized controlled trial with 48-hour follow-up*, Journal of Sport Rehabilitation, 2021, 30 (5), 697–706, DOI: 10.1123/jsr.2020-0183.

[15] DE ASLA R.J., KOZÁNEK M., WAN L., RUBASH H.E., LI G., *Function of anterior talofibular and calcaneofibular ligaments during in-vivo motion of the ankle joint complex*, Journal of Orthopaedic Surgery and Research, 2009, 4, 1–6, DOI: 10.1186/1749-799X-4-7.

[16] DUFEK J.S., BATES B.T., *Biomechanical factors associated with injury during landing in jump sports*, Sports Medicine, 1991, 12, 326–327, DOI: 10.2165/00007256-199112050-00005.

[17] FONG C.-M., BLACKBURN J.T., NORCROSS M.F., MCGRATH M., PADUA D.A., *Ankle-dorsiflexion range of motion and landing biomechanics*, Journal of Athletic Training, 2011, 46 (1), 5–10, DOI: 10.4085/1062-6050-46.1.5.

[18] GABRIEL M.T., WONG E.K., WOO S.L.Y., YAGI M., DEBSKI R.E., *Distribution of in situ forces in the anterior cruciate ligament in response to rotatory loads*, Journal of Orthopaedic Research, 2004, 22 (1), 85–89, DOI: 10.1016/S0736-0266(03)00133-5.

[19] GAO X., XU D., BAKER J.S., EE-CHON T., LIANG M., GU Y., *Exploring biomechanical variations in ankle joint injuries among Latin dancers with different stance patterns: utilizing OpenSim musculoskeletal models*, Frontiers in Bioengineering and Biotechnology, 2024, 12, 1359337, DOI: 10.3389/fbioe.2024.1359337.

[20] GARDINER J.C., WEISS J.A., ROSENBERG T.D., *Strain in the human medial collateral ligament during valgus loading of the knee*, Clinical Orthopaedics and Related Research, 2001, 391, 266–274, DOI: 10.1097/00003086-200110000-00031.

[21] GILLEN Z.M., JAHN L.E., SHOEMAKER M.E., MCKAY B.D., MENDEZ A.I., BOHANNON N.A., CRAMER J.T., *Effects of eccentric preloading on concentric vertical jump performance in youth athletes*, Journal of Applied Biomechanics, 2019, 35 (5), 327–335, DOI: 10.1123/jab.2018-0340.

[22] GIRON F., CUOMO P., AGLIETTI P., BULL A.M., AMIS A.A., *Femoral attachment of the anterior cruciate ligament*, Knee Surgery, Sports Traumatology, Arthroscopy, 2006, 14, 250–256, DOI: 10.1007/s00167-005-0685-y.

[23] GODEST A., BEAUGONIN M., HAUG E., TAYLOR M., GREGSON P., *Simulation of a knee joint replacement during a gait cycle using explicit finite element analysis*, Journal of Biomechanics, 2002, 35 (2), 267–275, DOI: 10.1016/S0021-9290(01)00179-8.

[24] Gu Y., Ren X., Li J., Lake M., Zhang Q., Zeng Y., *Computer simulation of stress distribution in the metatarsals at different inversion landing angles using the finite element method*, International Orthopaedics, 2010, 34, 669–676, DOI: 10.1007/s00264-009-0856-4.

[25] Hall E.A., Docherty C.L., *Validity of clinical outcome measures to evaluate ankle range of motion during the weight--bearing lunge test*, Journal of Science and Medicine in Sport, 2017, 20 (7), 618–621, DOI: 10.1016/j.jsams.2016.11.001.

[26] Halloran J.P., Petrella A.J., Rullkoetter P.J., *Explicit finite element modeling of total knee replacement mechanics*, Journal of Biomechanics, 2005, 38 (2), 323–331, DOI: 10.1016/j.jbiomech.2004.02.046.

[27] Haut Donahue T.L., Hull M., Rashid M.M., Jacobs C.R., *A finite element model of the human knee joint for the study of tibio-femoral contact*, J. Biomech. Eng., 2002, 124 (3), 273–280, DOI: 10.1115/1.1470171.

[28] Ho K.-Y., Blanchette M.G., Powers C.M., *The influence of heel height on patellofemoral joint kinetics during walking*, Gait and Posture, 2012, 36 (2), 271–275, DOI: 10.1016/j.gaitpost.2012.03.008.

[29] Hoch M.C., Farwell K.E., Gaven S.L., Weinhandl J.T., *Weight-bearing dorsiflexion range of motion and landing biomechanics in individuals with chronic ankle instability*, Journal of Athletic Training, 2015, 50 (8), 833–839, DOI: 10.4085/1062-6050-50.5.07.

[30] Hubley-Kozey C., Deluzio K., Dunbar M., *Muscle co-activation patterns during walking in those with severe knee osteoarthritis*, Clinical Biomechanics, 2008, 23 (1), 71–80, DOI: 10.1016/j.clinbiomech.2007.08.019.

[31] Kang Z., Jiang X., *The effect of running experience on muscle forces and knee joint reaction forces during running*, International Journal of Biomedical Engineering and Technology, 2024, 45 (3), 183–197, DOI: 10.1504/IJBET.2024.138969.

[32] Knörlein B.J., Baier D.B., Gatesy S.M., Laurence--Chasen J., Brainerd E.L., *Validation of XMALab software for marker-based XROMM*, Journal of Experimental Biology, 2016, 219 (23), 3701–3711, DOI: 10.1242/jeb.145383.

[33] Koyama T., Rikukawa A., Nagano Y., Sasaki S., Ichikawa H., Hirose N., *Acceleration profile of high-intensity movements in basketball games*, The Journal of Strength and Conditioning Research, 2022, 36 (6), 1715–1719, DOI: 10.1519/JSC.0000000000003699.

[34] Kubo K., Miyazaki D., Tanaka S., Shimoju S., Tsunoda N., *Relationship between Achilles tendon properties and foot strike patterns in long-distance runners*, Journal of Sports Sciences, 2015, 33 (7), 665–669, DOI: 10.1080/02640414.2014.962576.

[35] Lee J., Song Y., Shin C.S., *Effect of the sagittal ankle angle at initial contact on energy dissipation in the lower extremity joints during a single-leg landing*, Gait & Posture, 2018, 62, 99–104, DOI: 10.1016/j.gaitpost.2018.03.019.

[36] Leppänen M., Pasanen K., Krosshaug T., Kannus P., Vasankari T., Kujala U.M., Bahr R., Perttunen J., Parkkari J., *Sagittal plane hip, knee, and ankle biomechanics and the risk of anterior cruciate ligament injury: a prospective study*, Orthopaedic Journal of Sports Medicine, 2017, 5 (12), 2325967117745487, DOI: 10.1177/2325967117745487.

[37] LeRoux M.A., Setton L.A., *Experimental and biphasic FEM determinations of the material properties and hydraulic permeability of the meniscus in tension*, J. Biomech. Eng., 2002, 124 (3), 315–321, DOI: 10.1115/1.1468868.

[38] Li G., Lopez O., Rubash H., *Variability of a three-dimensional finite element model constructed using magnetic resonance images of a knee for joint contact stress analysis*, J. Biomech. Eng., 2001, 123 (4), 341–346, DOI: 10.1115/1.1385841.

[39] Li G., Van de Velde S.K., Bingham J.T., *Validation of a non--invasive fluoroscopic imaging technique for the measurement of dynamic knee joint motion*, Journal of Biomechanics, 2008, 41 (7), 1616–1622, DOI: 10.1115/1.1385841.

[40] Liu X., Zhang M., *Redistribution of knee stress using laterally wedged insole intervention: Finite element analysis of knee–ankle–foot complex*, Clinical Biomechanics, 2013, 28 (1), 61–67, DOI: 10.1016/j.clinbiomech.2012.10.004.

[41] Logerstedt D.S., Ebert J.R., MacLeod T.D., Heiderscheit B.C., Gabbett T.J., Eckenrode B.J., *Effects of and Response to Mechanical Loading on the Knee*, Sports Medicine, 2022, 52 (2), 201–235, DOI: 10.1007/s40279-021-01579-7.

[42] Malloy P., Morgan A., Meinerz C., Geiser C., Kipp K., *The association of dorsiflexion flexibility on knee kinematics and kinetics during a drop vertical jump in healthy female athletes*, Knee Surgery, Sports Traumatology, Arthroscopy, 2015, 23, 3550–3555, DOI: 10.1007/s00167-014-3222-z.

[43] Markovic G., Dizdar D., Jukic I., Cardinale M., *Reliability and factorial validity of squat and countermovement jump tests*, The Journal of Strength and Conditioning Research, 2004, 18 (3), 551–555, DOI: 10.1519/1533-4287(2004)18<551:RAFVOS>2.0.CO;2.

[44] Márquez G., Aguado X., Alegre L.M., Férnandez-del--Olmo M., *Neuromechanical adaptation induced by jumping on an elastic surface*, Journal of Electromyography and Kinesiology, 2013, 23 (1), 62–69, DOI: 10.1016/j.jelekin.2012.06.012.

[45] Marshall J., Bishop C., Turner A., Haff G.G., *Optimal training sequences to develop lower body force, velocity, power, and jump height: A systematic review with meta-analysis*, Sports Medicine, 2021, 51, 1245–12471, DOI: 10.1007/s40279-021-01430-z.

[46] Muneta T., Koga H., Nakamura T., Horie M., Watanabe T., Sekiya I., *Behind-remnant arthroscopic observation and scoring of femoral attachment of injured anterior cruciate ligament*, Knee Surgery, Sports Traumatology, Arthroscopy, 2016, 24, 2906–2914, DOI: 10.1007/s00167-015-3574-z.

[47] Norcross M.F., Almog R., Huang Y.-L., Chang E., Hannigan K.S., Johnson S.T., *Greater explosive quadriceps strength is associated with greater knee flexion at initial contact during landing in females*, Sports Biomechanics, 2024, 23 (8), 1028–1042, DOI: 10.1080/14763141.2021.1908413.

[48] Nuzzo J.L., McBride J.M., Cormie P., McCaulley G.O., *Relationship between counter movement jump performance and multijoint isometric and dynamic tests of strength*, The Journal of Strength & Conditioning Research, 2008, 22 (3), 699–707, DOI: 10.1080/14763141.2021.1908413.

[49] Ota S., Ueda M., Aimoto K., Suzuki Y., Sigward S., *Acute influence of restricted ankle dorsiflexion angle on knee joint mechanics during gait*, The Knee, 2014, 21 (3), 669–675, DOI: 10.1016/j.knee.2014.01.006.

[50] Pailler-Mattei C., Bec S., Zahouani H., *In vivo measurements of the elastic mechanical properties of human skin by indentation tests*, Medical Engineering and Physics, 2008, 30 (5), 599–606, DOI: 10.1016/j.medengphy.2007.06.011.

[51] Pena E., Calvo B., Martinez M., Doblare M., *A three-dimensional finite element analysis of the combined behavior of ligaments and menisci in the healthy human knee joint*, Journal of Biomechanics, 2006, 39 (9), 1686–1701, DOI: 10.1016/j.jbiomech.2005.04.030.

[52] Petrigna L., Karsten B., Marcolin G., Paoli A., D'Antona G., Palma A., Bianco A., *A review of counter-*

movement and squat jump testing methods in the context of public health examination in adolescence: reliability and feasibility of current testing procedures, Frontiers in Physiology, 2019, 10, 1384, DOI: 10.3389/fphys.2019.01384.

[53] PODRAZA J.T., WHITE S.C., *Effect of knee flexion angle on ground reaction forces, knee moments and muscle co-contraction during an impact-like deceleration landing: implications for the non-contact mechanism of ACL injury*, The Knee, 2010, 17 (4), 291–295, DOI: 10.1016/j.knee.2010.02.013.

[54] POWDEN C.J., HOCH J.M., HOCH M.C., *Reliability and minimal detectable change of the weight-bearing lunge test: a systematic review*, Manual Therapy, 2015, 20 (4), 524–532, DOI: 10.1016/j.math.2015.01.004.

[55] SANNA G., O'CONNOR K.M., *Fatigue-related changes in stance leg mechanics during sidestep cutting maneuvers*, Clinical Biomechanics, 2008, 23 (7), 946–954, DOI: 10.1016/j.clinbiomech.2008.03.065.

[56] SETH A., HICKS J.L., UCHIDA T.K., HABIB A., DEMBIA C.L., DUNNE J.J., ONG C.F., DEMERS M.S., RAJAGOPAL A., MILLARD M., *OpenSim: Simulating musculoskeletal dynamics and neuromuscular control to study human and animal movement*, PLoS Computational Biology, 2018, 14 (7), e1006223, DOI: 10.1371/journal.pcbi.1006223.

[57] SIEGLER S., BLOCK J., SCHNECK C.D., *The mechanical characteristics of the collateral ligaments of the human ankle joint*, Foot and Ankle, 1988, 8 (5), 234–242, DOI: 10.1177/107110078800800502.

[58] SONG Y., DEBSKI R.E., MUSAHL V., THOMAS M., WOO S.L.-Y., *A three-dimensional finite element model of the human anterior cruciate ligament: a computational analysis with experimental validation*, Journal of Biomechanics, 2004, 37 (3), 383–390, DOI: 10.1016/S0021-9290(03)00261-6.

[59] SUGGS J., WANG C., LI G., *The effect of graft stiffness on knee joint biomechanics after ACL reconstruction – a 3D computational simulation*, Clinical Biomechanics, 2003, 18 (1), 35–43, DOI: 10.1016/S0268-0033(02)00137-7.

[60] VAN EIJDEN T., DE BOER W., WEIJS W., *The orientation of the distal part of the quadriceps femoris muscle as a function of the knee flexion-extension angle*, Journal of Biomechanics, 1985, 18 (10), 803–809, DOI: 10.1016/0021-9290(85)90055-7.

[61] WANG H.-K., CHEN C.-H., SHIANG T.-Y., JAN M.-H., LIN K.-H., *Risk-factor analysis of high school basketball–player ankle injuries: A prospective controlled cohort study evaluating postural sway, ankle strength, and flexibility*, Archives of Physical Medicine and Rehabilitation, 2006, 87 (6), 821–825, DOI: 10.1016/j.apmr.2006.02.024.

[62] WIKSTROM E.A., TILLMAN M.D., CHMIELEWSKI T.L., BORSA P.A., *Measurement and evaluation of dynamic joint stability of the knee and ankle after injury*, Sports Medicine, 2006, 36, 393–410, DOI: 10.2165/00007256-200636050-00003.

[63] WILCZYŃSKI B., ZORENA K., ŚLĘZAK D., *Dynamic knee valgus in single-leg movement tasks. Potentially modifiable factors and exercise training options. A literature review*, International Journal of Environmental Research and Public Health, 2020, 17 (21), 8208, DOI: 10.3390/ijerph17218208.

[64] XU D., LU J., BAKER J.S., FEKETE G., GU Y., *Temporal kinematic and kinetics differences throughout different landing ways following volleyball spike shots*, Proceedings of the Institution of Mechanical Engineers, Journal of Sports Engineering and Technology, 2022, 236 (3), 200–208, DOI: 10.1177/17543371211009485.

[65] XU D., QUAN W., ZHOU H., SUN D., BAKER J.S., GU Y., *Explaining the differences of gait patterns between high and low-mileage runners with machine learning*, Scientific Reports, 2022, 12 (1), 2981, DOI: 10.1038/s41598-022-07054-1.

[66] XU D., ZHOU H., QUAN W., GUSZTAV F., BAKER J.S., GU Y., *Adaptive neuro-fuzzy inference system model driven by the non-negative matrix factorization-extracted muscle synergy patterns to estimate lower limb joint movements*, Computer Methods and Programs in Biomedicine, 2023, 242, 107848, DOI: 10.1016/j.cmpb.2023.107848.

[67] XU D., ZHOU H., QUAN W., GUSZTAV F., WANG M., BAKER J.S., GU Y., *Accurately and effectively predict the ACL force: Utilizing biomechanical landing pattern before and after-fatigue*, Computer Methods and Programs in Biomedicine, 2023, 241, 107761, DOI: 10.1016/j.cmpb.2023.107761.

[68] XU D., ZHOU H., WANG M., MA X., GUSZTAV F., CHON T.-E., FERNANDEZ J., BAKER J.S., GU Y., *Contribution of ankle motion pattern during landing to reduce the knee-related injury risk*, Computers in Biology and Medicine, 2024, 180, 108965, DOI: 10.1016/j.compbiomed.2024.108965.

[69] XU D., ZHOU H., QUAN W., MA X., CHON T.-E., FERNANDEZ J., GUSZTAV F., KOVÁCS A., BAKER J.S., GU Y., *New insights optimize landing strategies to reduce lower limb injury risk*, Cyborg and Bionic Systems, 2024, 5, 0126, DOI: 10.34133/cbsystems.0126.

[70] XU D., ZHOU H., QUAN W., JIANG X., LIANG M., LI S., UGBOLUE U.C., BAKER J.S., GUSZTAV F., MA X., *A new method proposed for realizing human gait pattern recognition: Inspirations for the application of sports and clinical gait analysis*, Gait & Posture, 2024, 107, 293–305, DOI: 10.1016/j.gaitpost.2023.10.019.

[71] YAN M., LIANG T., ZHAO H., BI Y., WANG T., YU T., ZHANG Y., *Model Properties and Clinical Application in the Finite Element Analysis of Knee Joint: A Review*, Orthopaedic Surgery, 2024, 16 (2), 289–302, DOI: 10.1111/os.13980.

[72] YEOW C.H., LEE P.V.S., GOH J.C.H., *An investigation of lower extremity energy dissipation strategies during single-leg and double-leg landing based on sagittal and frontal plane biomechanics*, Human Movement Science, 2011, 30 (3), 624–635, DOI: 10.1016/j.humov.2010.11.010.

[73] ZHANG Q., ZHANG Y., CHON T.E., BAKER J.S., GU Y., *Analysis of stress and stabilization in adolescent with osteoporotic idiopathic scoliosis: Finite element method*, Computer Methods in Biomechanics and Biomedical Engineering, 2023, 26 (1), 12–24, DOI: 10.1080/10255842.2022.2044803.

[74] ZHANG S.-N., BATES B.T., DUFEK J.S., *Contributions of lower extremity joints to energy dissipation during landings*, Medicine and Science in Sports and Exercise, 2000, 32 (4), 812–819, DOI: 10.1097/00005768-200004000-00014.

[75] ZHANG Z., XU D., GAO X., LIANG M., BAKER J.S., GU Y., *The Effect of Different Degrees of Ankle Dorsiflexion Restriction on the Biomechanics of the Lower Extremity in Stop-Jumping*, Applied Bionics and Biomechanics, 2024, 2024 (1), 9079982, DOI: 10.1155/2024/9079982.

[76] ZHOU H., UGBOLUE U.C., *Biomechanical analysis of lower limbs based on unstable condition sports footwear: a systematic review*, Physical Activity and Health, 2024, 8 (1), DOI: 10.5334/paah.332.

[77] ZHOU H., XU D., QUAN W., UGBOLUE U.C., GU Y., *Effects of different contact angles during forefoot running on the stresses of the foot bones: a finite element simulation study*, Frontiers in Bioengineering and Biotechnology, 2024, 12, 1337540, DOI: 10.3389/fbioe.2024.1337540.

[78] ZHOU H., XU D., CHEN C., UGBOLUE U.C., BAKER J.S., GU Y., *Analysis of different stop-jumping strategies on the biomechanical changes in the lower limbs*, Applied Sciences, 2021, 11 (10), 4633, DOI: 10.3390/app11104633.

[79] ZHOU H., XU D., QUAN W., UGBOLUE U.C., ZHOU Z., GU Y., *Can the entire function of the foot Be concentrated in the forefoot area during the running stance phase? A finite element study of different shoe soles*, Journal of Human Kinetics, 2023, 92, 5, DOI: 10.5114/jhk/174311.

[80] ZHOU Z., ZHOU H., JIE T., XU D., TEO E.-C., WANG M., GU Y., *Analysis of stress response distribution in patients with lateral ankle ligament injuries: a study of neural control strategies utilizing predictive computing models*, Frontiers in Physiology, 2024, 15, 1438194, DOI: 10.3389/fphys.2024.1438194.